Spatial Composition Grading of Quaternary ZnCdSSe Alloy Nanowires with Tunable Light Emission between 350 and 710 nm on a Single Substrate

Anlian Pan,[†] Ruibin Liu, Minghua Sun, and Cun-Zheng Ning*

School of Electrical, Computer and Energy Engineering and Center of Nanophotonics, Arizona State University, Tempe, Arizona 85287. [†]On leave from Key Laboratory for Micro-Nano Optoelectronic Devices of Ministry of Education, and Micro-Nanotechnology Research Center, Hunan University, Changsha 410082, China.

ABSTRACT We demonstrated a general methodology of growing spatially composition-controlled alloys by combining spatial source reagent gradient with a temperature gradient. Using this *dual gradient* method, we achieved for the first time a continuous spatial composition grading of single-crystal quaternary $Zn_xCd_{1-x}S_ySe_{1-y}$ alloy nanowires over the complete band gap range along the length of a substrate. The band gap grading spans between 3.55 eV (ZnS) and 1.75 eV (CdSe) on a single substrate, with the corresponding light emission over the entire visible spectrum. We also showed that the dual gradient method can be extended to achieve alloy composition control in two spatial dimensions. The unique material platform achieved will open a wide range of applications from color engineered display and lighting, full spectrum solar cells, multispectral detectors, or spectrometer on-a-chip to superbroadly tunable nanolasers. The growth methodology can be extended more generally to other alloy systems.

KEYWORDS: quaternary alloys · composition grading · semiconductor · nanowires · tunable · single substrate · visible spectrum · dual gradient method

Band gaps are one of the most important parameters of semiconductor materials for optoelectronic applications since they determine the spectral features of absorptions and emission processes. Due to the limited band gaps of natural semiconductors (such as elementary semiconductors or binary compounds), alloying different semiconductors becomes one of the major methods of realizing new band gaps, but this method is also limited by the lattice mismatch between the substrate and the alloy materials to be grown using the planar epitaxial growth methods. Nanomaterials such as nanowires open a new vista of band gaps through alloying with almost arbitrary compositions.[1−29] While different band gaps have been achieved through alloy composition changes by *separate growths*, it is more important for many applications to be able to produce all possible band gaps on a single substrate with spatial controlled distributions, such as a controlled spatial grading of band gaps through composition grading. Composition-graded alloy semiconductor nanostructures on a single chip can work as a material platform for a wide range of applications from superbroadly tunable nanolasers, through color engineered display and lighting, and multispectral detectors to full spectrum solar cells. More specifically in a photovoltaic device, spatial composition-controlled alloy materials can potentially allow band gaps tailored to match the full solar spectrum for maximum conversion efficiency.[30] Spatial alloy composition engineering and control can lead to on-chip direct white light generation for solid state lighting or color design for display applications. In detectors, multispectral detection or spectrometer on-a-chip has been envisaged as an ultimate mode of detection. Widely tunable semiconductor lasers are another technologically important application of single-chip-based semiconductor alloys. Despite such well-recognized applications, the lack of growth and fabrication technology for such materials has long been the main bottleneck.

Recently, we successfully realized a one-dimensional (1D) composition grading in the full alloy composition range of ternary CdSSe nanowires on a single substrate through the temperature gradient control in a CVD system and achieved spatially continuously tunable lasing with a wavelength tuning range of 200 nm, unmatched by any other available semiconductor-based laser.[9] Using a different approach, full composition range of ternary InGaN nanowires was also achieved for the first time through a spatial gradient of reactants during the

*Address correspondence to cning@asu.edu.

Received for review August 25, 2009 and accepted January 07, 2010.

Published online January 14, 2010.
10.1021/nn901699h

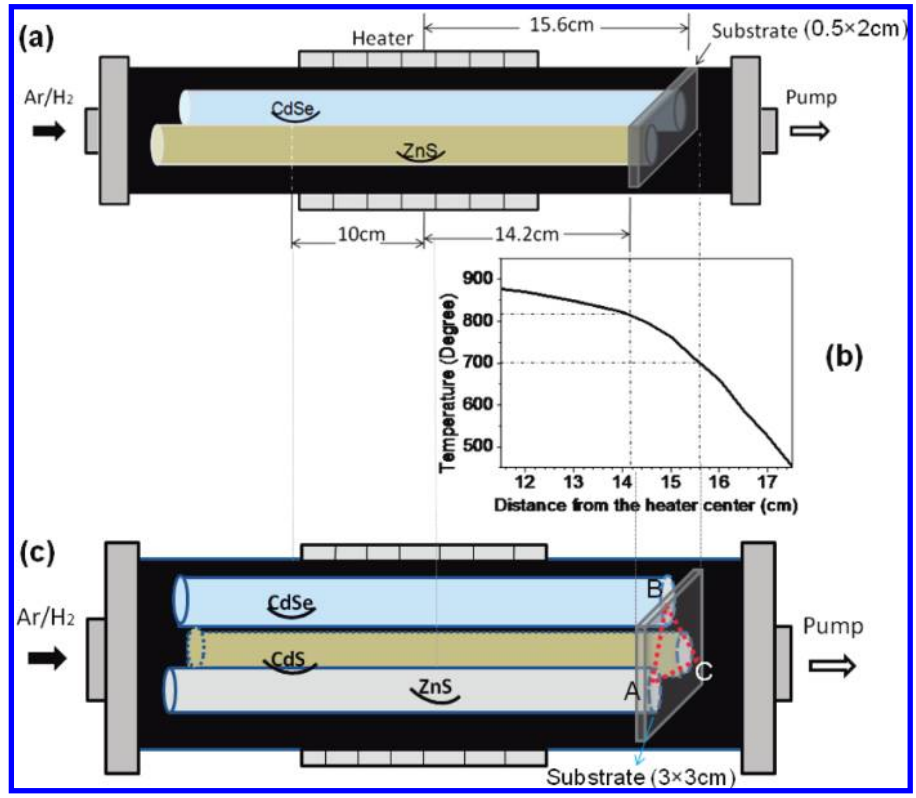

Figure 1. (a) Setup and tube configuration for the growth of the 1D graded sample, (b) temperature profile at the sample growth zone, and (c) setup and tube configuration for the growth of the 2D graded sample.

CVD growth.[4] In a more recent paper,[29] we were able to achieve for the first time quaternary alloy nanobelts with different compositions covering the entire visible spectrum through Au-catalyzed vapor−liquid−solid (VLS) growth route. While this result was very encouraging, different alloy compositions (thus colors) were produced by *separate* growths. These results,[4,9,29] while achieving unprecedented alloy material capabilities, also indicate great potential and flexibility of a more general strategy in growing alloy nanowire materials with a well-controlled spatial composition distribution. The purposes of this paper are as follows: (1) to present a more general strategy of growing composition-graded alloy nanowires/belts; (2) to produce the entire band gap range of ZnCdSSe (corresponding to the entire visible spectrum) on a single substrate in a *single* run of growth for the first time; and (3) to demonstrate the spatial control of alloy composition in two spatial dimensions.

RESULTS AND DISCUSSION

For the purposes described above, we designed a new CVD growth configuration by combining the temperature gradient[9] with the spatial reaction reagent gradient.[4] This general methodology is called dual gradient method (DGM) hereafter. We successfully achieved a continuous spatial 1D composition grading of quaternary $Zn_xCd_{1-x}S_ySe_{1-y}$ alloy semiconductor nanowires, with a fine band gap tunability from 3.55 eV (ZnS) to 1.75 eV (CdSe) (corresponding to the entire visible spectrum) on a single substrate. This general strategy of combining spatial reagent gradient and temperature gradient for growing composition grading of alloy nanomaterials is also extended to achieve alloy composition control in two space dimensions (2D). The experimental setups and growth conditions are schematically shown in Figure 1.

Figure 2A shows the real-color photograph under room lighting of the as-grown 1D composition-graded sample, where color changes from dark (on the ZnS side) to white (on the CdSe side). The same sample under a UV laser illumination along the central stripe shows much richer colors from red through yellow, green and blue to purple (see Figure 2B), indicating band gap gradual change along the substrate length. Figure $2C_1-C_5$ shows the scanning electron microscopy (SEM) images from five representative points taken in turn from the white ZnS-rich end to the dark CdSe-rich end along the length of the sample. The SEM result indicates that most of the substrate is covered by nanowires with diameters of 100−200 nm and lengths of several tens of micrometers, while the product changes to tapered nanobelts with mean width of 1−2 μm toward the CdSe-rich end. Figure $2D_1-D_5$ shows representative TEM images of single nanostructures from samples shown in Figure $2C_1-C_5$, respectively. Each of them has a gold catalyst at the tip, indicating the VLS growth mechanism of these alloy nanostructures. The *in situ* EDS (see Figure $2E_1-E_5$, respectively) from these single wires shows that all of the wires contain elements Zn, S,

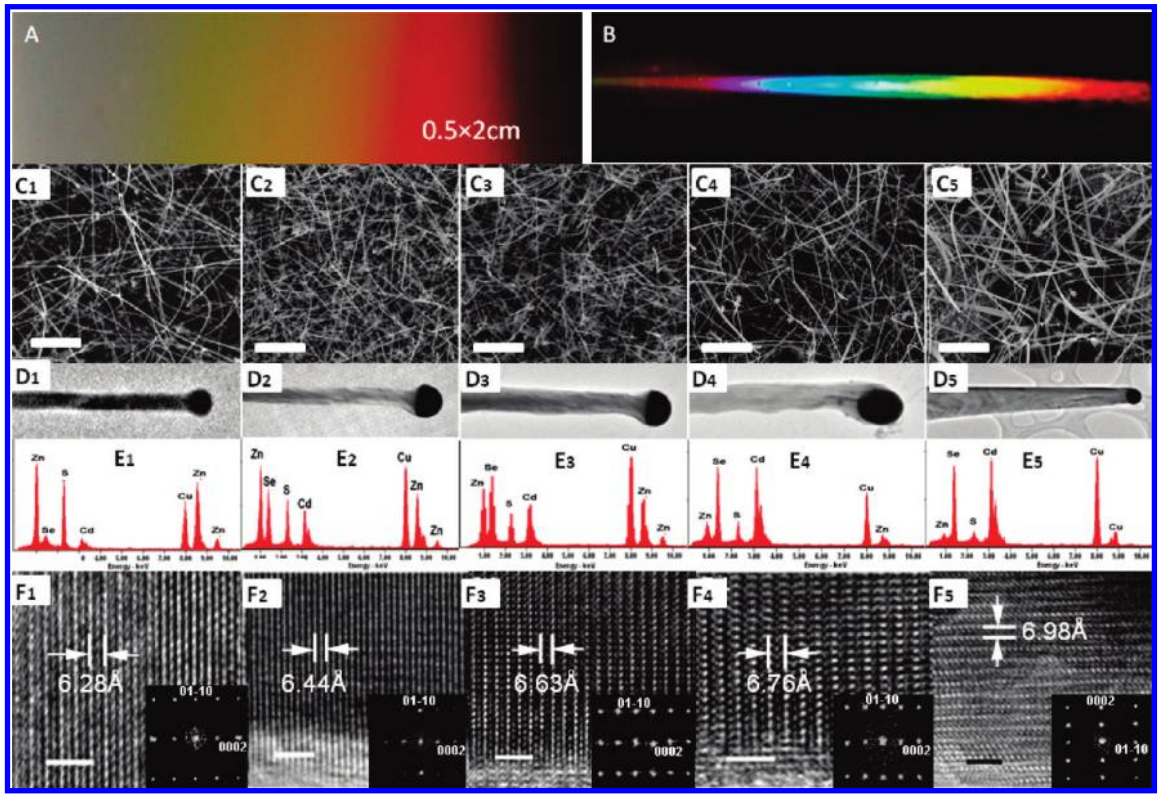

Figure 2. (A,B) Real-color photograph of the as-grown sample with 1D composition grading under room lighting and under a UV laser (266 nm) illumination along the central stripe, respectively. (C_1−C_5) SEM images from five representative points collected in turn from the white ZnS-rich end to the dark CdSe-rich end along the length of the sample, respectively. Scale bar: 5 μm. (D_1−D_5) Representative TEM images of single wires from samples A_1 to E_1, respectively; (E_1−E_5) corresponding *in situ* EDS from these single wires. (F_1−F_5) Corresponding HRTEM images of these single wires shown in D_1−D_5, respectively. Insets: the corresponding FFT patterns. Scale bar: 2 nm.

Cd, and Se (element Cu is from the copper grid), and the Cd−Se concentrations are complementary to those of Zn and S along the length of the substrate. The high-resolution TEM (HRTEM) images of these wires shown in Figure 2F_1−F_5 as well as the corresponding fast Fourier transform (FFT) patterns (see the insets) indicate the single-crystal nature and wurtzite hexagonal structure of the wires. The measured (0001) interplanar spacing gradually increases from samples F_1 to F_5, which is in agreement with the increment of composition Cd and Se and is also consistent with the observed color change of the sample (see Figure 2A,B). The TEM results demonstrate that the obtained sample consists of composition-tunable quaternary ZnCdSSe nanostructures.

The change of morphology from wire-like to belt-like toward the CdSe end of the sample indicates different growth kinetics. During the VLS growth process, the gas-phase supersaturation of the atoms or molecules of the growing material has important effects on the morphology of the obtained nanostructures.[31] Low level of supersaturation favors the growth of wires or rod-like structures, while high supersaturation benefits the formation of quasi-2D belt-like structures.[31] For these spatially graded ZnCdSSe alloys, their relative compositions of Zn−S to Cd−Se are mainly decided by the respective evaporation and deposition of ZnS and CdSe sources. Since the melting point of ZnS powder (~1830 °C) is much higher than that of CdSe powder (~1350 °C), the evaporation rate of ZnS is much lower than that of CdSe during the growth. This was seen in the experiments when CdSe powder was fully consumed after the growth, while most of ZnS powder remains. The low supersaturation or vapor pressure due to the slow evaporation of ZnS favors the 1D nucleation and the growth of wire-like structures using the VLS mechanism. While the rapid evaporation of CdSe produces very high supersaturation or vapor pressure of CdSe, leading to the 2D nucleation and the growth of belt-like structures near the CdSe end.

We used small-area X-ray diffraction (XRD) to further examine the position-dependent crystal quality/structure across the overall length of the sample. Figure 3a shows the XRD mapping of the wires along the length of the sample with a step of 2 mm. The standard 2θ values for ZnS and CdSe wurtzite single crystals are also shown for comparison. The XRD results show that all the wires have wurtzite hexagonal crystal structure and are consistent with the TEM measurements. The relatively weaker intensities toward the ZnS-rich end come from the thinner depth of wire materials and the very small scanning area of the XRD measurements. The diffraction peaks shift gradually from the ZnS-rich end to the CdSe-rich end toward

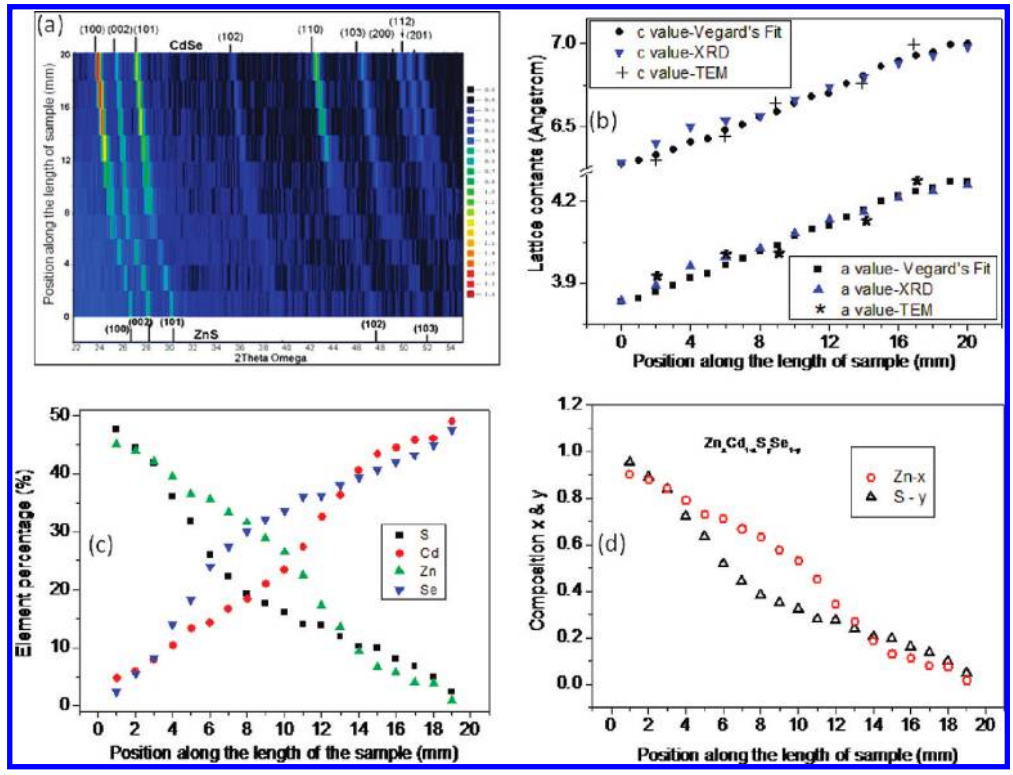

Figure 3. (a) Spatial XRD scan along the length of the 1D composition-graded sample with a step of 2 mm, as well as the standard 2θ values for ZnS and CdSe wurtzite single crystals. (b) Position-dependent lattice constants *a* and *c*, along the length of the sample obtained from the fitting of XRD data (blue triangles), the Vegard law approximation (dark filled circles and rectangles), and the TEM measurements (crosses and stars). (c) Element profiles along the length of the 1D graded sample, (d) the corresponding converted position-dependent composition *x* and *y*.

smaller angles, indicating the formation of alloys with intermediate compositions with their lattice constants gradually increased. Figure 3b shows the position-dependent lattice constants *a* and *c*, along the length of the sample. The blue triangles show the values extracted from the XRD data. The dark filled circles and rectangles show the Vegard law approximation for the quaternary alloys,[32−36] using the lattice constants of the four binary compounds: ZnS, ZnSe, CdS, and CdSe. The composition variables, *x* and *y*, are determined from the element profile measurements of the sample (shown in Figure 3c,d). The crosses and stars denote the values from the TEM measurements. The very good agreement among the results from these three independent avenues establishes the spatial composition-graded quaternary alloys on the as-grown sample.

The position-dependent normalized photoluminescence (PL) spectra (Figure 4a) show that every spot along the length of the substrate has a single-peak light emission, and that the peak wavelength is tuned gradually from near UV (~350 nm) at the ZnS-rich end to ~710 nm at the CdSe-rich end, covering the entire visible region. This spectral change is consistent with the color range shown under the UV light illumination (Figure 2B). The position/composition-tunable PL indicates that the emitted light comes from the band-edge emission of the alloys. No other defect-related emission band was found across the whole sample, indicative of the high crystal quality of the alloy wires. Figure 4b shows the composition *x*-dependent PL peak energy along the sample (empty triangles) and the alloy band gap values (filled circles) interpolated using the following standard interpolation formula for quaternary semiconductor alloys $A_xB_{1-x}C_yD_{1-y}$:[37]

$$E_g(A_xB_{1-x}C_yD_{1-y}) = E_g(AC)xy + E_g(BD)(1-x)(1-y) + E_g(BC)(1-x)y + E_g(AD)x(1-y) \quad (1)$$

For quaternary $Zn_xCd_{1-x}S_ySe_{1-y}$, $E_g(AC)$, $E_g(BD)$, $E_g(BC)$, and $E_g(AD)$ are the band gap values of ZnS (3.6 eV), ZnSe (2.8 eV), CdS (2.44 eV), and CdSe (1.72 eV), respectively. Using the position−composition relation along the sample (see Figure 3c,d), we also obtained the position-dependent PL peak energy and the interpolated band gap values (shown in Figure 4c). The good agreement shown in Figure 4b,c between the PL peak energy and the bandgap values is a further validation of the spatial one-to-one correspondence between alloy composition and band gaps (or PL peak energies). The little deviation at the ZnS-rich end (high *x* value) mainly comes from the interpolation formula we used. An additional bowling item in eq 1 is expected to reduce the deviations between the PL and the fitting. Other contributing factors to the slight disagreement can come from measurement precisions. The overall agreement together with all the other compositional and structural

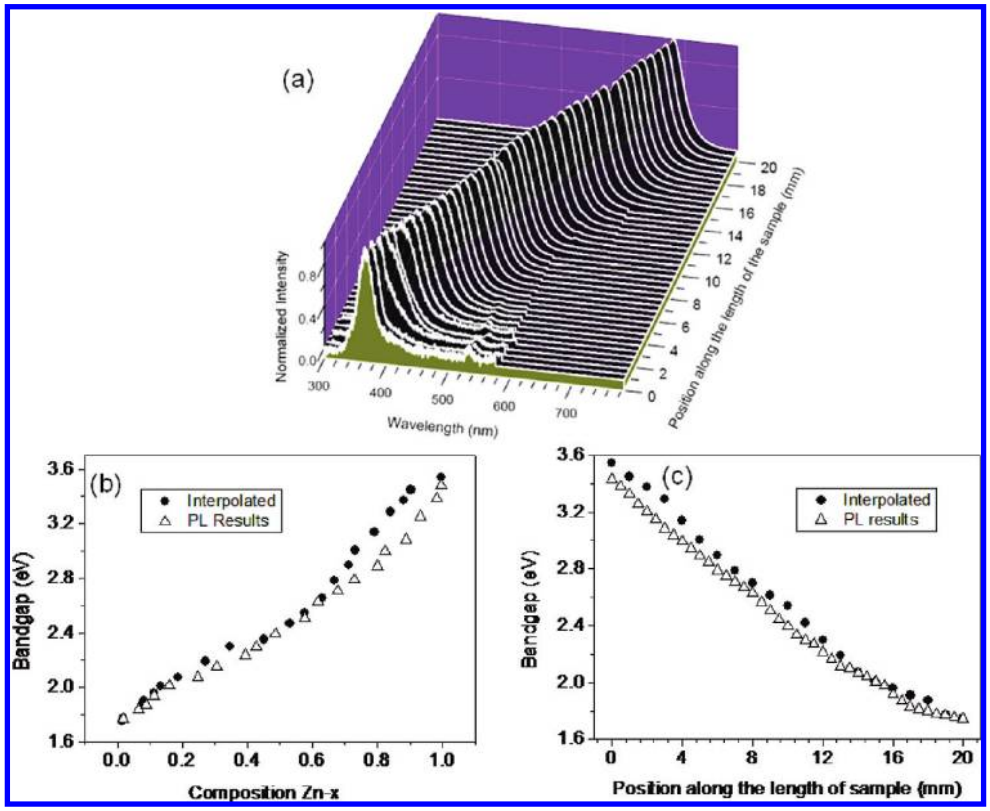

Figure 4. (a) Position-dependent PL spectra (normalized) along the length of the 1D sample; (b) composition *x*-dependent PL peak energy (empty triangles) and the alloy band gap values interpolated using the standard interpolation formula for quaternary semiconductor (filled circles); (c) position-dependent PL peak energy (empty triangles) and interpolated band gap values (filled circles).

characterizations unambiguously demonstrates our realization of quaternary alloy nanowires and their spatial controlled grading.

The success of the 1D composition grading indicates a more general strategy of engineering the alloy composition in 2D and in a controllable fashion. Figures 5a shows the real-color photograph of the as-grown 2D graded sample under UV light illumination, grown using the setup with three mini-tubes arranged in an equilateral triangle (see Figure 1c). Positions A, B, and C in Figure 5a are close to the downstream ends of the mini-tubes loaded with ZnS, CdSe, and CdS powder, respectively. Figure 5b−d shows that the respective element profiles along the three sides of the indicated triangle shown in Figure 5a,e−g are the corresponding converted composition *x* and *y* with position along the sides of the triangle. These spatial compositional results combined with the SEM observations (not shown here) indicate that the whole substrate range is also composed of quaternary ZnCdSSe nanowires. As a result, this photograph (Figure 5a) exhibits a 2D color map produced by the spatial graded composition in the plane of the substrate.

Figure 6a−c shows the normalized PL spectra of the 2D graded sample along each side of the triangle ABC, respectively, and Figure 6d gives the corresponding position-dependent peak wavelength/energy along the triangle. Just as in the case of the 1D graded alloys, the PL spectra from every spot along the sides of the triangle all show strong single-peak band-edge emission, with their peak wavelength tunable with the position.

Figure 7 is a convenient way of expressing the $Zn_xCd_{1-x}S_ySe_{1-y}$ quaternary alloys in their two-dimensional composition plane. The four corners represent the four possible binaries, ZnS, ZnSe, CdS, and CdSe, while the four edges represent the corresponding four ternaries with varying composition. The interior points (*x*,*y*) of this composition square represent quaternary alloys of possible compositions. Typically, a given composition (a point in this plane) is grown in a specific planar epitaxial growth. Here for the two-dimensional spatial composition grading, the composition scan along an arbitrary path of the substrate reveals a particular composition dependence, which corresponds to a specific curve in the composition plane. The 1D graded sample (see Figure 2A) has a fixed composition (*x*,*y*) dependence corresponding to one curve in the composition plane (shown as green stars in Figure 7). The 2D graded sample can have many different composition dependences or curves in the composition plane, depending on the scanning path. As representatives, the compositional dependences for the scanning along the three sides of the triangle are given as black rectangles, red circles, and blue triangles, respectively, in Figure 7. It is interesting to point out that many com-

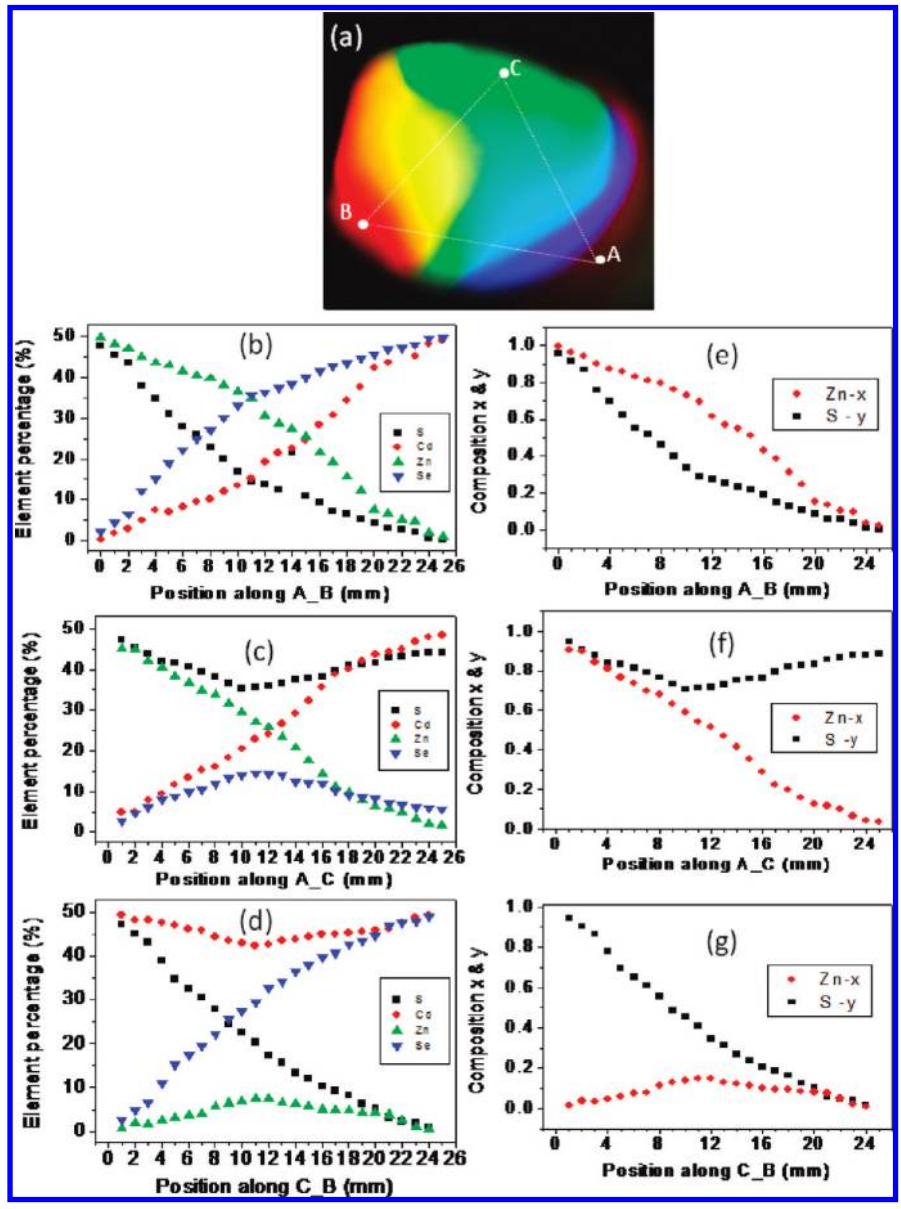

Figure 5. (a) Real-color photograph of the sample with 2D composition grading under UV light illumination. Positions A, B, and C in (a) are close to the downstream ends of the mini-tubes loaded with ZnS, CdSe, and CdS powder, respectively. (b−d) Element profiles along the three sides of the indicated triangle shown in (a), respectively, and (e−g) corresponding converted composition *x* and *y* with position.

position dependences or curves in this plane can be achieved by a single run of growth of our two-dimensional graded samples. It would be also very interesting to map the entire substrate into this composition square, providing a unique platform for studying the quaternary alloys more generally with various compositions.

As shown above, the spatial compositional distribution of the ZnCdSSe alloys on the substrate can be achieved over the entire band gap range by the spatial configurations of the multichannel growth system together with the proper temperature profile to produce the dual gradients in the growth zone. We emphasize that our dual gradient method is crucial for achieving such a spatial quaternary composition grading with high crystal quality. The spatial configured mini-tubes provide multichannels of different reagent vapors to be transported to the different spatial areas of the substrate to form source reagent gradient, and the controlled temperature gradient allows different source vapors (ZnS, CdS, and CdSe) to be deposited at different locations with optimized local temperatures. The demonstration of the DGM is an important aspect of this work, and we believe that this DGM can be used as a general strategy to grow other alloy systems and to achieve much more complicated spatial composition engineering. We have performed comprehensive parametric study with only one of the gradients. The results show that either gradient alone cannot achieve the complete band gap range of the ZnCdSSe from that of

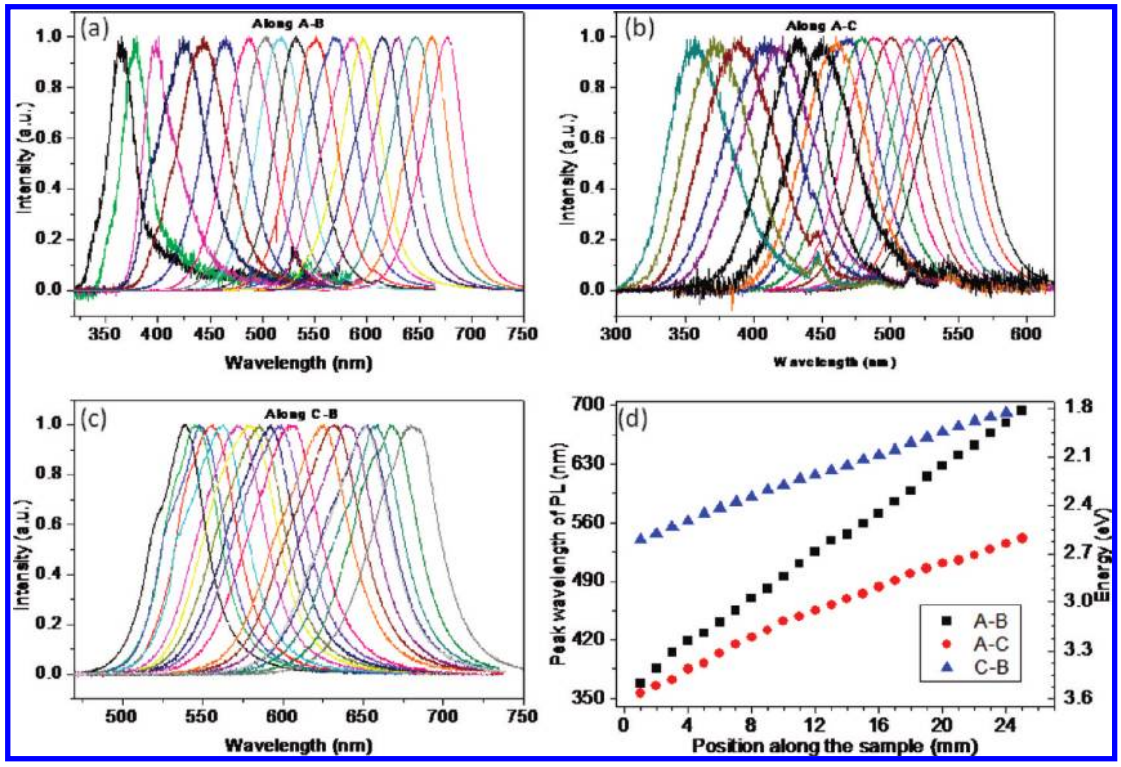

Figure 6. (a−c) Normalized spectra of the 2D graded sample along each side of the triangle ABC, respectively, and (d) the corresponding position-dependent PL peak wavelength/energy along the triangle.

ZnS to that of CdSe with high crystal quality on a single substrate.

Figure 8a−c shows the real-color photographs under the regular room lighting of the three samples obtained when the substrate was placed perpendicular to the tube axis at a uniform temperature of 700, 760, and 810 °C, respectively. The corresponding element scans along the three sides of triangle ABC are shown to the right side of each photograph. The results clearly show that the sample grown at 700 °C has very little Zn, and the sample grown at 810 °C is composed mainly of Zn and S. A detailed composition examination shows that none of the three samples can have the entire quaternary composition range between $Zn_1Cd_0S_1Se_0$ ($x = 1$, $y = 1$) and $Zn_0Cd_1S_0Se_1$ ($x = 0$, $y = 0$) along any scanning path. In other words, reagent gradient alone is not sufficient for achieving the complete quaternary spatial composition grading. In addition, the reagent gradient alone with uniform substrate temperature very often produces nanomaterials with poor crystal quality with wide PL spectrum or strong midgap emissions, especially at the regions with wide gap materials. This is true for the growth of spatial composition-graded nanowires of both ternary and quaternary alloys. Similarly, our extensive experiments also show that the temperature gradient alone without the reagent gradient produced by the multiple mini-tubes is also not sufficient to grow quaternary alloy with a wide range of composition grading, even though composition-graded ternary alloys such as ZnCdS or CdSSe can be grown successfully. Proper spatial separation of different reagent elements enabled by the properly configured multiple tubes is essential to grow the complete quaternary composition grading.

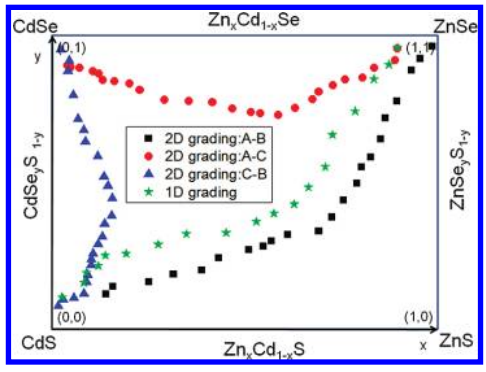

Figure 7. The compositional $x-y$ relations for the 1D composition graded sample (green stars), and the 2D graded sample along the three sides of the triangle ABC (black rectangles, red circles, and blue triangles), respectively.

Using the dual gradient method demonstrated in this paper, the spatial composition grading or control can be more easily achieved by varying the diameters and the spatial configuration of the mini-tubes and by the tilting angles of the substrate which determine the temperature gradient on the substrate. At the same time, the spatial composition profiles can be affected by the relative evaporation rates of the sources. In the experiments, we used quite low evaporation temperature compared to the melting points of the source materials, thus the vapor pressure and thus the composition of the achieved alloys can be controlled mainly by the dual gradient mentioned without the need of ad-

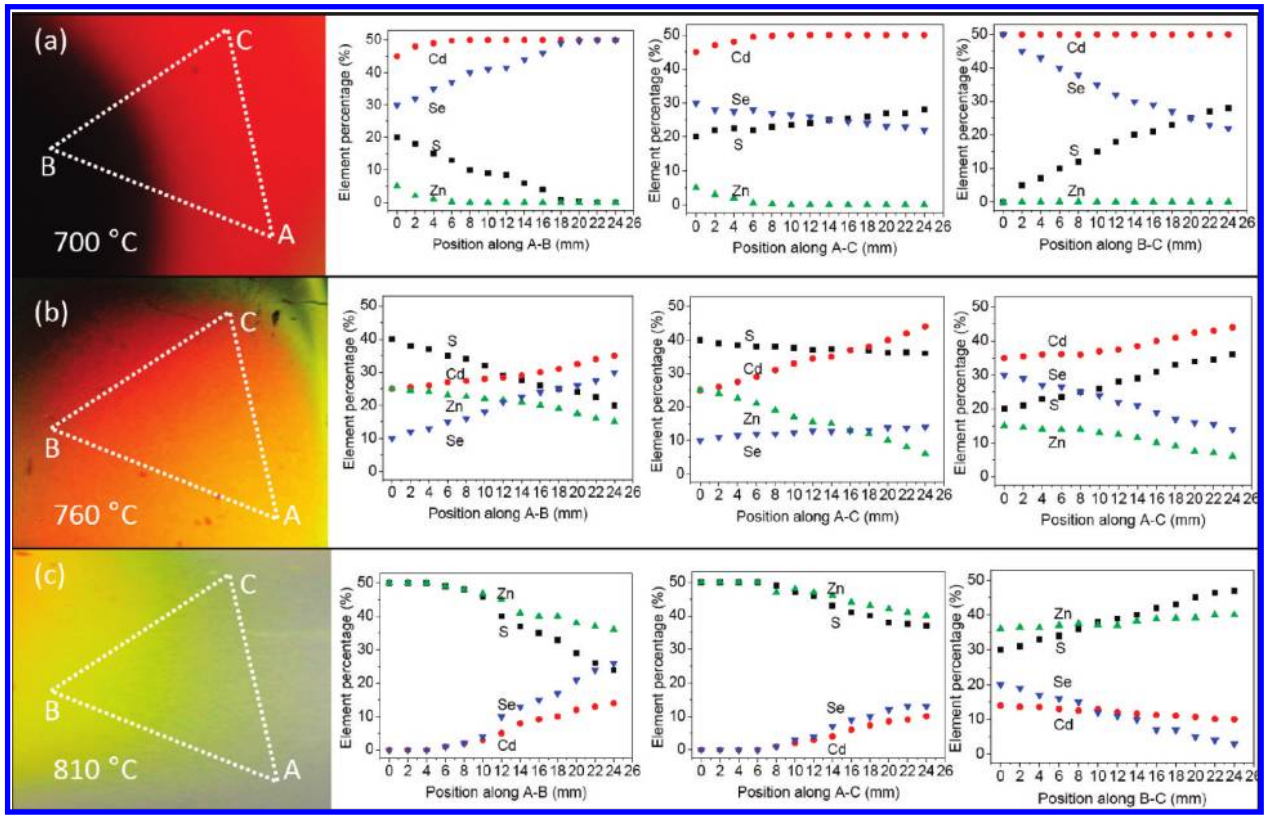

Figure 8. (a−c) Real-color photographs under room lighting of the samples obtained when the substrate was placed perpendicular to the tube axis at a local temperature of 700, 760, and 810 °C, respectively. The three panels at the right of each photograph are the corresponding element profiles along the three sides of the indicated triangle ABC.

justing the ratio of sources. Such dual gradient approach has produced ZnCdSSe quaternary alloys in the entire band gap range with high crystal quality, and this general strategy can be used to achieve spatially controlled semiconductor alloy nanostructures of other material systems.

CONCLUSIONS

We demonstrated a general methodology, the dual gradient method, of growing spatially composition-controlled alloys by the combination of the spatial source reagent gradient method[4] and the temperature gradient method.[9] Even though such gradient methods were used separately for growing ternary alloys, we show that the combination of the two is a more general approach and necessary for growing quaternary alloys and even high quality ternary alloys. Using the DGM, we achieved a continuous spatial grading of single-crystal quaternary $Zn_xCd_{1-x}S_ySe_{1-y}$ alloy nanowires with continuous composition tunability along the length of a substrate, leading to a continuous band gap change from 3.55 eV (ZnS) to 1.75 eV (CdSe) (corresponding to the entire visible spectrum) on a single substrate. We also showed that our approach can be extended to achieve alloy composition control in two spatial dimensions. Since alloys of different alloy compositions in general require different deposition temperatures, only spatial source materials profiling through mini-tube configuration are not sufficient to grow high quality nanowires. The inclusion of temperature gradient is essential so that this method can be used more generally to produce spatially controlled alloy composition variations in other alloy systems. Such composition-controlled alloy nanowires on a single substrate provide a unique material platform for a wide range of applications from color engineered display and lighting, full spectrum solar cells, multispectral detectors, or spectrometer on-a-chip to superbroadly tunable nanolasers.

EXPERIMENTAL SECTION

Sample Synthesis. Experimental growth of quaternary ZnCdSSe nanowires with spatial composition grading was conducted through an improved CVD route in the presence of Au as a catalyst. For the growth of the 1D graded sample, two 1/4 in. diameter quartz mini-tubes were placed horizontally inside a 1 in. diameter quartz tube for transporting the reaction reagents independently to the reaction zone. Before growth, appropriate amounts of high-purity ZnS and CdSe source powders (Alfa Aesar, 99.995%) were loaded into the two mini-tubes separately. ZnS powder was positioned at the center of the furnace, while CdSe powder was placed upstream of the furnace center. A piece of quartz (0.5 × 2 cm in size) presputtered with 2 nm of Au film

was positioned downstream facing the ends of the mini-tubes. The substrate was tilted into a proper angle, such that its two ends are at different axial locations with different temperatures. The tube reactor was evacuated and back-flushed with Ar/H_2-5% gas until the desired pressure of 15 Torr was reached. A constant flow of 50 sccm was used during growth. The temperature at the furnace center was set to 940 °C, with a heating rate of 40 °C/min, and maintained at its peak temperature for 2 min. During the growth, the vapors coming from the two neighboring mini-tubes will spread and interdisperse along the length of the substrate, thus forming spatial composition-graded alloys on the substrate. As an example of 2D graded sample, the outside tube was replaced with a 1.5 in. diameter quartz tube, and an additional mini-tube with the same size was added inside the big tube for loading CdS powder with the three tubes forming an equal-side triangle. The CdS powder was placed at the same longitudinal position as the CdSe powder. The previous rectangular substrate (for 1D grading) was replaced by a square one of 3 × 3 cm in size. As in the case of 1D grading, the square substrate was also tilted, so that the end of the ZnS-carrying tube points to the higher temperature side of the substrate. All other growth conditions are the same as those for the 1D grading. See Figure 1 for the schematically experimental setups and growth conditions.

Structural Characterizations. Scanning electron microscopy (SEM) images and the *in situ* energy-dispersive X-ray spectroscopy (EDS) analysis were performed using a Philips XL-30 field-emission SEM equipped with an energy-dispersive X-ray detector. To determine the elemental composition at each point on the sample, the substrate was accurately positioned using an encoded $x-y$ translation stage, and the locations were recorded. The background-subtracted Zn (L), Cd (L), Se (L), and S (K) lines were analyzed using the standard-less quantification mode of the energy-dispersive X-ray analysis software. Transmission electron microscopy (TEM) images were collected with a JEOL JEM-2010 high-resolution transmission electron microscopy at 200 kV, equipped with a Link EDS detector. The nanowires from each of the examined areas along the substrate were carefully picked up with a needlepoint under an optical microscope. Small-area X-ray diffraction (XRD) data were collected on the PANalytical X'Pert Pro Materials Research X-ray diffractometer equipped with a Cu Kα radiation (λ = 1.54178 Å). The focused X-ray beam (~0.5 mm) scanned automatically along the length of the sample, with a regular interval of 2 mm.

Optical Measurements. Room-temperature PL studies of the graded samples were conducted using a pulsed (6 ns, 10 Hz) frequency-quadrupled Nd:YAG laser (Spectra Physics Quanta Ray, at 266 nm) as the pump source. The pump beam was focused by a 250 mm focal length lens to a spot size of ~300 μm on the sample at an incidence angle of ~43°. Luminescence from the samples was then collected by a Mitutoyo objective lens (Plan APO, SL, 100×), placed normal to the sample. The collected light was directed to a 0.3 m spectrometer and detected with a liquid nitrogen cooled CCD detector. The spatial resolution and spectral resolution were estimated to be ~700 and 0.2 nm, respectively. The samples were scanned across the length (for the 1D graded sample) or along any selected paths (for the 2D graded sample) of the substrate to accurately measure the position-dependent light emission.

To take the color picture of the as-grown 1D graded sample under UV laser illumination, the laser beam was diffused into a strip using a cylindrical lens, illuminating the total length of the sample; for that of the 2D graded sample, the laser beam was diffused into a large circle using a diffusing lens, simultaneously illuminating a large part of the central area of the sample.

Acknowledgment. The authors thank the U.S. Army Research Office for financial support and D. Wright of the Center of Solid State Science at ASU for his technical help with the CVD system.

REFERENCES AND NOTES

1. Huang, Y.; Duan, X. F.; Lieber, C. M. Semiconductor Nanowire for Multi-Color Photonics. *Small* **2005**, *1*, 142–147.
2. Duan, X. F.; Lieber, C. M. General Synthesis of Compound Semiconductor Nanowires. *Adv. Mater.* **2000**, *12*, 298–302.
3. Qian, F.; Li, Y.; Gradecak, S.; Park, H.; Dong, Y.; Ding, Y.; Wang, Z. L.; Lieber, C. M. Multi-Quantum-Well Nanowire Heterostructures for Wavelength-Controlled Lasers. *Nat. Mater.* **2008**, *7*, 701–706.
4. Kyukendall, T.; Ulrich, P.; Aloni, S.; Yang, P. Complete Composition Tunability of InGaN Nanowires Using a Combinatorial Approach. *Nat. Mater.* **2007**, *6*, 951–956.
5. Pan, A. L.; Yang, H.; Liu, R.; Yu, R.; Zou, B.; Wang, Z. L. Color-Tunable Photoluminescence of Alloyed CdS_xSe_{1-x} Nanobelts. *J. Am. Chem. Soc.* **2005**, *127*, 15692–15693.
6. Xu, H.; Liang, Y.; Liu, Z.; Zhang, X.; Hark, S. Synthesis and Optical Properties of Tetrapod-like ZnSSe Alloy Nanostructures. *Adv. Mater.* **2008**, *20*, 3294–3297.
7. Wang, M.; Fei, G. T.; Zhang, Y. G.; Kong, M. G.; Zhang, L. D. Tunable and Predetermined Bandgap Emissions in Alloyed ZnS_xSe_{1-x} Nanowires. *Adv. Mater.* **2007**, *19*, 4491–4494.
8. Hua, B.; Motohisa, J.; Kobayashi, Y.; Hara, S.; Fukui, T. Single GaAs/GaAsP Coaxial Core−Shell Nanowire Lasers. *Nano Lett.* **2009**, *9*, 112–116.
9. Pan, A. L.; Zhou, W.; Leong, E. S. P.; Liu, R.; Chin, A. H.; Zou, B.; Ning, C. Z. Continuous Alloy-Composition Spatial Grading and Superbroad Wavelength-Tunable Nanowire Lasers on a Single Chip. *Nano Lett.* **2009**, *9*, 784–788.
10. Pan, A.; Wang, X.; He, P.; Zhang, Q.; Wan, Q.; Zacharias, M.; Zhu, Xing.; Zou, B. Color-Changeable Optical Transport through Se-Doped CdS 1D Nanostructures. *Nano Lett.* **2007**, *7*, 2970–2975.
11. Liu, Y.; Zapien, J. A.; Shan, Y. Y.; Geng, C. Y.; Lee, C. S.; Lee, S. T. Wavelength Controlled Lasing in $Zn_xCd_{1-x}S$ Single Crystal Nanoribbons. *Adv. Mater.* **2005**, *17*, 1372–1377.
12. Boykin, T. B.; Luisier, M.; Schenk, A.; Kharche, N.; Klimeck, G. The Electronic Structure and Transmission Characteristics of Disordered AlGaAs Nanowires. *IEEE Trans. Nanotechnol.* **2007**, *6*, 43–47.
13. Lim, S. K.; Tambe, M. J.; Brewster, M. M.; Gradecak, S. Controlled Growth of Ternary Alloy Nanowires Using Metalorganic Chemical Vapor Deposition. *Nano Lett.* **2008**, *8*, 1386–1392.
14. Su, J.; Gherasimova, M.; Cui, G.; Tsukamoto, H.; Han, J.; Onuma, T.; Kurimoto, M.; Chichibu, S. F.; Broadbridge, C. Growth of AlGaN Nanowires by Metalorganic Chemical Vapor Deposition. *Appl. Phys. Lett.* **2005**, *87*, 183108/1–183108/3.
15. Liu, Y. K.; Zapien, J. A.; Shan, Y. Y.; Tang, H.; Lee, C. S.; Lee, S. T. Wavelength-Tunable Lasing in Single-Crystal $CdS_{1-x}Se_x$ Nanoribbons. *Nanotechnology* **2007**, *18*, 365606/1–365606/7.
16. Hsu, H. C.; Wu, C. Y.; Cheng, H. M.; Hsieh, W. F. Band Gap Engineering and Stimulated Emission of ZnMgO Nanowires. *Appl. Phys. Lett.* **2007**, *89*, 013101–013103.
17. Zapien, J.; Liu, Y.; Shan, Y.; Tang, H.; Lee, C.; Lee, S. T. Continuous Near-Infrared-to-Ultraviolet Lasing from II−VI Nanoribbons. *Appl. Phys. Lett.* **2007**, *90*, 213114–213116.
18. Kwon, S. J.; Choi, Y. J.; Park, J. H.; Hwang, I. S.; Park, J. G. Structural and Optical Properties of CdS_xSe_{1-x} Nanowires. *Phys. Rev. B* **2005**, *72*, 205312/1–205312/7.
19. Zhai, T.; Zhang, X.; Yang, W.; Ma, Y.; Wang, J.; Gu, Z.; Yu, D.; Yang, H.; Yao, J. Growth of Single Crystalline $Zn_xCd_{1-x}S$ Nanocombs by Metallo-Organic Chemical Vapor Deposition. *Chem. Phys. Lett.* **2006**, *427*, 371–374.
20. Zhou, S. M.; Feng, Y. S.; Zhang, L. D. Growth and Optical Characterization of Large-Scale Crystal $Cd_xZn_{1-x}S$ Whiskers *via* Vapor Reaction. *J. Cryst. Growth* **2003**, *252*, 1–3.
21. Persson, A. I.; Bjork, M. T.; Jeppesen, S.; Wagner, J. B.; Wallenberg, L. R.; Samuelson, L. $InAs_{1-x}P_x$ Nanowires for Device Engineering. *Nano Lett.* **2006**, *6*, 403–407.
22. Shan, C. X.; Liu, Z.; Ng, C. M.; Hark, S. K. $Zn_xCd_{1-x}Se$ Alloy Nanowires Covering the Entire Compositional Range Grown by Metalorganic Chemical Vapor Deposition. *Appl. Phys. Lett.* **2005**, *87*, 033108/1–033108/3.
23. Venugopal, R.; Lin, P.; Chen, Y. T. Photoluminescence and Raman Scattering from Catalytically Grown $Zn_xCd_{1-x}Se$ Alloy Nanowires. *J. Phys. Chem. B* **2006**, *110*, 11691–11696.

24. Lorenz, M.; Kaidashev, E. M.; Rahm, A.; Nobis, T.; Lenzner, J.; Wagner, G.; Spemann, D.; Hochmuth, H.; Grundmann, M. $Mg_xZn_{1-x}O$ ($0 \leq x < 0.2$) Nanowire Arrays on Sapphire Grown by High-Pressure Pulsed-Laser Deposition. *Appl. Phys. Lett.* **2005**, *86*, 143113/1–143113/3.
25. Kling, R.; Kirchner, C.; Gruber, T.; Reuss, F.; Waag, A. Analysis of ZnO and ZnMgO Nanopillars Grown by Self-Organization. *Nanotechnology* **2004**, *15*, 1043–1046.
26. Pan, A.; Yao, L.; Qin, Y.; Yang, Y.; Kim, D. S.; Yu, R.; Zou, B.; Werner, P.; Zacharias, M.; Goesele, U. Si−CdSSe Core/Shell Nanowires with Continuously Tunable Light Emission. *Nano Lett.* **2008**, *8*, 3413–3417.
27. Bhattacharyya, S.; Estrin, Y.; Moshe, O.; Rich, D. H.; Solovyov, L. A.; Gedanken, A. Highly Luminescent $Zn_xCd_{1-x}Se$/C Core/Shell Nanocrystals: Large Scale Synthesis, Structural and Cathodoluminescence Studies. *ACS Nano* **2009**, *3*, 1864–1876.
28. Rincon, M. E.; Martinez, M. W.; Miranda-Hernandez, M. Structural, Optical and Photoelectrochemical Properties of Screen-Printed and Sintered $(CdS)_x(ZnS)_{1-x}$ ($0 < x < 1$) Films. *Sol. Energy Mater. Sol. Cells* **2003**, *77*, 25–40.
29. Pan, A.; Liu, R.; Sun, M.; Ning, C. Quaternary Alloy Semiconductor Nanobelts with Bandgap Spanning the Entire Visible Spectrum. *J. Am. Chem. Soc.* **2009**, *131*, 9502–9503.
30. Ning, C.; Pan, A.; Liu, R. Spatially Composition-Graded Alloy Semiconductor Nanowires and Wavelength Specific Lateral-Multijunction Full-Spectrum Solar Cells. Proceedings of the 34th IEEE PVSC June, 2009 pp 001492−001495.
31. Ye, C. H.; Fang, X. S.; Hao, Y. F.; Teng, X. M.; Zhang, L. D. Zinc Oxide Nanostructures: Morphology Derivation and Evolution. *J. Phys. Chem. B* **2005**, *109*, 19758–19765.
32. Feng, Y. P.; Teo, K. L.; Lim, F.; Poon, H. C.; Ong, C. K.; Xia, J. B. Empirical Pseudopotential Band-Structure Calculation for $Zn_xCd_{1-x}S_ySe_{1-y}$ Quaternary Alloy. *J. Appl. Phys.* **1993**, *74*, 3948–3955.
33. Vijayalakshmi, R. P.; Venugopal, R.; Reddy, D. R.; Reddy, B. K. Structural and Bandgap Studies of ZnSCdSe Thin Films. *Semicond. Sci. Technol.* **1994**, *9*, 1062–1068.
34. Marques, M. Statistical Model Applied to $A_xB_yC_{1-x-y}D$ Quaternary Alloys: Bond Lengths and Energy Gaps of $Al_xGa_yIn_{1-x-y}X$ (X = As, P, or N) Systems. *Phys. Rev. B* **2006**, *73*, 232205/1–232205/8.
35. Kim, K.; Zunger, A. Spatial Correlations in GaInAsN Alloys and Their Effects on Band-Gap Enhancement and Electron Localization. *Phys. Rev. Lett.* **2001**, *86*, 2609–2612.
36. Nahory, R. E; Pollack, M. A.; Johnston, W. D.; Barns, R. L. Band Gap *versus* Composition and Demonstration of Vegard's Law for $In_{1-x}Ga_xAs_yP_{1-y}$ Lattice Matched to InP. *Appl. Phys. Lett.* **1978**, *33*, 659–661.
37. Tamargo, M. C. *II-VI Semiconductor Materials and their Applications*; Taylor & Francis: New York, 2002.